Ultra-high granularity electromagnetic calorimetry – Results from the EPICAL-2 prototype and perspectives for digital calorimeters

T. Peitzmann[1,*], *J.* Alme[2], *R.* Barthel[1], *V.* Borshchov[3,4], *R.* Bosley[5], *A.* van den Brink[1], *H.* Buesching[6], *O.S.* Groettvik[2,**], *J.* Keul[6], *N.* van der Kolk[1,7], *O.* Kravchenko[3], *Q.W.* Malik[8], *F.* Pliquett[6], *M.* Protsenko[3,4], *K.* Røed[8], *T.* Rogoschinski[6], *D.* Röhrich[2], *M.* Rossewij[1], *J.* Schoengarth[6], *E.H.* Solheim[8], *I.* Tymchuk[3,4], *K.* Ullaland[2], *N.K.* Watson[5], and *H.* Yokoyama[1,7]

[1]Institute for Gravitational and Subatomic Physics (GRASP), Utrecht University/Nikhef, Utrecht, Netherlands
[2]Department of Physics and Technology, University of Bergen, Bergen, Norway
[3]Research and Production Enterprise "LTU" (RPE LTU), Kharkiv, Ukraine
[4]Bogolyubov Institute for Theoretical Physics, Kyiv, Ukraine
[5]University of Birmingham, Birmingham, United Kingdom
[6]Institut für Kernphysik, Johann Wolfgang Goethe-Universität Frankfurt, Frankfurt, Germany
[7]Nikhef, National Institute for Subatomic Physics, Amsterdam, Netherlands
[8]Department of Physics, University of Oslo, Oslo, Norway

Abstract. An advanced prototype of a digital pixel calorimeter, EPICAL-2, has been constructed using ALPIDE MAPS sensors. It has been successfully tested with cosmic muons and with test beams at DESY and the CERN SPS. We will report on recent updates of performance results, with good linearity and resolution. Comparisons to detailed MC simulations are made and show good understanding of the technology. The spatial precision of event-by-event measurements of the showers allows unprecedented studies of the shower shape. The detector features two-shower separation capabilities at extremely small distances. We will also discuss the limitations of the currently used sensor technology and perspectives for future development of digital calorimetry.

1 Introduction

A new type of SiW electromagnetic calorimeter is being developed using digital pixel sensors. The R&D is performed in the context of the FoCal upgrade [1] within the ALICE experiment and is related to studies of imaging in proton CT [2]; it is applicable to other future collider projects such as EIC, ILC, CLIC or FCC. Based on a proof of principle with a first digital calorimeter prototype [3], we have constructed an advanced second prototype, EPICAL-2, using ALPIDE MAPS sensors [4]. Binary readout is possible due to the pixel size of $\approx 30 \times 30\,\mu\text{m}^2$. The prototype consists of alternating W absorber of 3 mm thickness and Si sensor layers (24 layers in total), with a total thickness of $20X_0$, an area of 30mm × 30mm, and 25 million pixels.

Measurements with this prototype have been performed in an electron beam at DESY and a mixed beam at the CERN SPS. This paper will present results obtained from electrons (positrons) in an energy range from 1 – 80 GeV. Detailed simulations have been performed with the Allpix^2 simulation framework [5] based on GEANT4.

A more detailed description of the prototype, the analysis procedures and earlier results can be found in [6, 7].

*e-mail: t.peitzmann@uu.nl
**Now at European Organization for Nuclear Research (CERN), Geneva, Switzerland.

2 Energy response and linearity

The basic principle of a digital calorimeter is to use counting of shower particles as the energy response. In a first step one therefore has to identify observables providing this information. In a silicon pixel sensor such as the ALPIDE, every charged particle traversing it will produce electron-hole pairs in the silicon, which are transported through diffusion and drift, and finally are collected by the pixel diodes. In the transport, charges in general spread over the area of several pixels. Every pixel that receives an amount of charges above a given threshold generates a *hit*, such that a shower particle produces a *cluster* of several hits. The mean value of the thresholds is 82e. Both the number of hits (N_{hits}) and the number of clusters (N_{clus}) should on average be proportional to the number of shower particles, and can be used as response observables.

Figure 1 shows on the left the mean values of N_{hits}, N_{clus}, and the number of electrons/positrons N_e producing charges in the sensors, as obtained from simulations for different energies E of incident particles. To good approximation, all observables increase linearly with E. The values obtained for N_{clus} are very close to those of N_e. The values of N_{hits}, however, are significantly larger, which is a consequence of cluster size larger than 1.

All observables have been fitted with a linear function of the form $f(E) = cE$. No constant offset is expected in

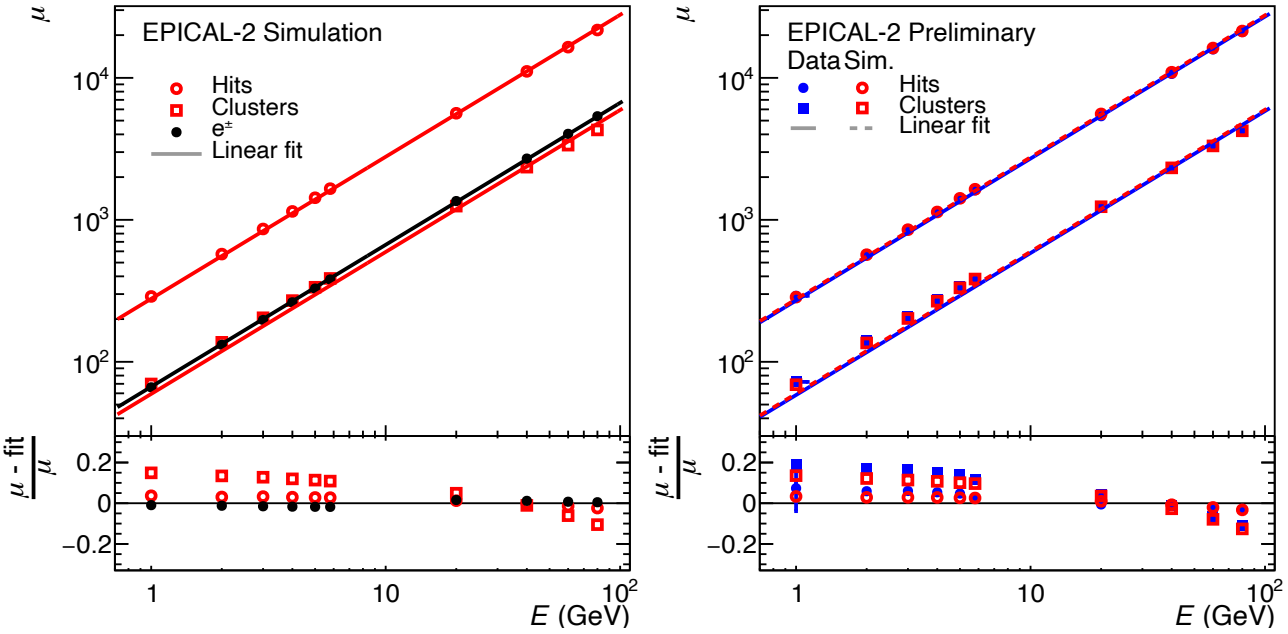

Figure 1. Mean value of different response observables as a function of beam energy. Left: Simulation results only, including the number of $e^{\pm}$ crossing the sensor layers. Right: Results from experimental data compared to simulations. All data sets are fitted with linear functions (see text), and the ratio of data point deviations to the fits is displayed in the bottom panels.

this dependence as the noise of the sensors is negligible. The fits follow the behaviour of the data, however, more subtle deviations can be seen from the ratios of the data points to the fit values, which are displayed in the bottom panel. For N_e, which is the ideal response observable for such a device, the mean values follow the proportionality very closely, the deviation is < 1%. The behaviour of N_{hits} is also very close to linear, with a deviation of up to a few %, while N_{clus} deviates by more than 10%.

The deviation from linearity in the two realistic observables is mostly due to overlap of hits or clusters due to the high particle density. Because a merging of clusters occurs already at relatively low density, when clusters are just directly adjacent and the number of hits is not affected, N_{clus} is much more sensitive to this effect leading to the stronger non-linearity.

The linearity behaviour of the response has also been studied from measured data, where N_e is obviously not available. The results are shown on the right of figure 1 together with the corresponding results from simulations. Overall, data and simulations show very similar behaviour. In the bottom panel which shows the deviations in a ratio, qualitatively similar deviations are seen, with the largest effects for N_{clus}. There is also a small discrepancy between measured data and simulations – in particular at low energies, the non-linearity appears to be stronger in measured data for both observables. We have identified this as most likely being due to a small bias in the true average beam energy of the DESY test beam [6] – taking this into account, the agreement between measurements and simulations is very good, supporting the interpretation of the results.

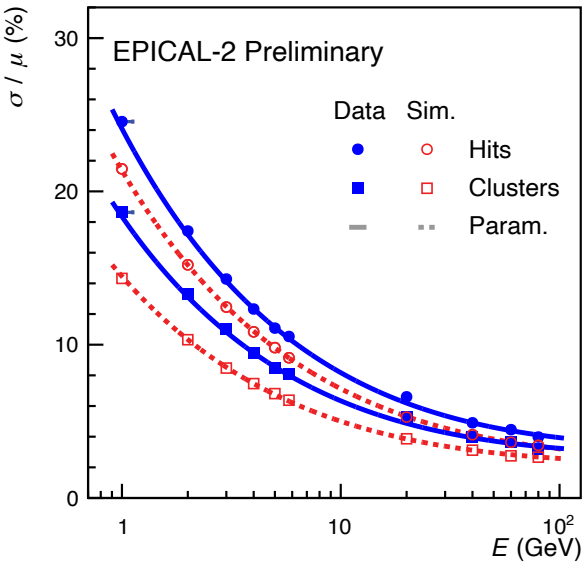

Figure 2. Relative energy resolution using either hits or clusters as a function of beam energy. Experimental data (blue) are compared to simulation (red). Fits of a parameterisation with equation 1 are also shown.

3 Energy resolution

From the distributions of N_{hits} and N_{clus} the resolution has been determined as the numerical standard deviation. The results for the relative resolution are displayed in figure 2. All data sets show the expected decrease of the resolution

with increasing energy, and a parameterisation of the form:

$$\frac{\sigma_E}{E} = \frac{a}{\sqrt{E/\mathrm{GeV}}} \oplus b \tag{1}$$

has been fitted, which describes the data well.

For the resolution, N_{clus} shows a better performance with lower values than N_{hits}. This is also observed in simulations, with both observables showing lower resolution values in simulations compared to data. This is not unexpected, as several experimental effects have not been implemented in the simulations, e.g. the energy spread of the incoming beam particles and the effect of the varying and possibly fluctuating values of the pixels thresholds in the sensors. Still, a good resolution is obtained also in measured data, in particular for N_{clus}. The parameterisation of equation (1) yields values of $a = (18.16 \pm 0.02)\%$ and $b = (2.68 \pm 0.03)\%$ in this case. One should note that due to some experimental effects which are not corrected, this is an upper limit for the true resolution.

4 Shower shape and lateral width

The very high granularity of the detector allows us to study the shower shape in unprecedented detail. As an example, the hit density per area A as a function of radial distance from the shower center:

$$\rho_{\mathrm{hits}}(r) = \frac{dN_{\mathrm{hits}}}{dA}(r) \tag{2}$$

is shown in figure 3 on the left for a beam energy of 40 GeV. The corresponding cluster density is not studied here, because the latter is distorted significantly due to saturation effects, which are most important in the core, leading to a broadening of the distributions. Some of the global features of the hit density distributions are expected: The total amplitude per layer, most accurately obtained as the integral of the distributions, increases up to layer 7, which is close to shower maximum, and then decreases again. In layer 7, the hit density in the inner core of the shower reaches values that approach the upper limit, the *saturation density* of $N_{\mathrm{hits}}^{\mathrm{max}} \approx 1272\,\mathrm{mm}^{-2}$.

The distributions are very narrow in early layers, and broaden the deeper the shower penetrates into the detector. However, even for the most narrow distributions in layer 2, i.e. at a depth of $z/X_0 \approx 1.7$, a tail of the distributions out to almost twice the value of the expected Molière radius is seen – the Molière radius expected from the material composition of the detector is $R_M \approx 10.85\,\mathrm{mm}$. It should be noted, that this tail is observable only due to the fact that the effective dynamic range of the local amplitude (the hit density) is larger than 10^5 in this low noise environment, a unique feature of this technology.

It is also interesting, that the simulation describes the distributions very well, even out to the tails.

As one way of characterising the shower shape for different layers and energies, the width in terms of the FWHM has been obtained. This is displayed in figure 3 on the right side. It gives a more quantitative expression of the features discussed above and also shows their energy dependence. In layer 2, the FWHM of the shower is of the order of 200 μm almost independent of beam energy. In layer 7, which is in the vicinity of the shower maximum for the higher energies, the FWHM is of the order of a mm at low energies and decreases to $\approx$ 400 μm at high energies. In layer 12, which is already in the longitudinal tail of the shower, there is a stronger energy dependence, but only a slightly larger value of the width at high energy. Finally, in layer 18, the shower is significantly broader, and in particular at low energies, significant fluctuations make the interpretation of the width more difficult.

5 Discussion and Conclusion

Good calorimetric performance is obtained with this prototype of a digital calorimeter. Two response observables, N_{clus} and N_{hits} have been used, and they exhibit distinct features.

1. N_{clus} shows stronger deviations from linearity but a better resolution.

2. N_{hits} shows better linearity but a worse resolution.

The ideal observable would be the true number of shower particles N_e, as studied above in simulations. N_{clus} gets closest to this ideal measure in a low density environment. Under these circumstances, the additional fluctuations of the cluster size worsen the resolution for N_{hits}.

For the behaviour of the average value, these additional fluctuations are not so relevant – the average cluster size is $\approx$ 5 and to good approximation independent of the beam energy. Here, the effect of saturation for high density is more important, and, as mentioned above, N_{clus} is more sensitive to this. Saturation sets in at densities where clusters touch each other and two or more clusters merge to one. At this same density, hits are not yet affected – they will only suffer significantly at much higher density.

In addition, detailed studies of the shower shape have been performed. Here, only the lateral shape is studied with radial distributions of the hit density per layer, which is possible down to a spatial resolution of $\approx 100\mu$m. It has been demonstrated, that the width of the shower quantified as the FWHM is of the order of a mm or smaller, in particular for early layers and reasonably high particle energy. The same pixel technology will be used for the high-granularity layers of the FoCal detector in ALICE, and their main task is the two-shower separation. The study presented here demonstrates that a two-shower separation on the level of a few mm, as required for FoCal, will be possible with this technology.

More studies of the shower shape, including the longitudinal distribution, are being studied and will be the subject of an upcoming publication.

The results obtained so far also yield important information for the future development of a digital calorimeter. At the energies studied here, the apparent non-linearity for N_{clus} is small enough to not spoil the performance. This response observable can still be used with a simple correction factor for the non-linearity. As saturation is, however, expected to increase strongly with increasing particle energy, the non-linearity will become intolerable above

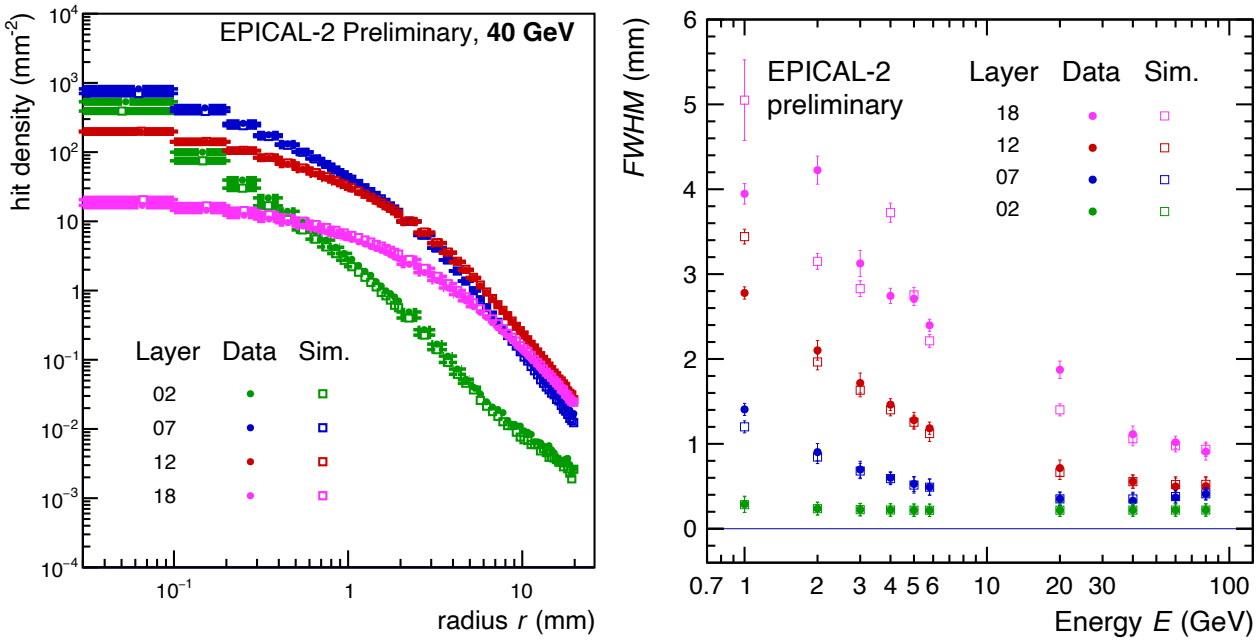

Figure 3. Left: Area density of hits as a function of radial distance from the shower center for a few selected layers for measured data (filled circles) and simulations (open squares) at a beam energy of 40 GeV. Right: Width (FWHM) of the lateral density distributions as a function of energy for a few selected layers. Both measured data and simulations are shown.

some energy, and this response observable will be unusable. Modifications will be necessary to keep the advantage of low resolution, or even attempt to further improve it. To achieve this, modifications that make the sensors more saturation-resistant will have to be employed. A further decrease of the pixel size, which would be a possible remedy, may not be realistic. Rather, one should probably consider to give the pixels some low-resolution amplitude capabilities, i.e. a conversion of the charge to a few bits instead of just one, as in the current design.

Such design changes should ideally go hand in hand with other updates improving the digital performance of the sensors. Beneficial for the use of this technology in a future collider experiment would be higher rate capabilities, data reduction customised for calorimeter use and possibilities for triggering.

References

[1] ALICE collaboration, Technical Design Report of the ALICE Forward Calorimeter (FoCal). CERN-LHCC-2024-004 (2024). https://cds.cern.ch/record/2890281

[2] J. Alme, et al., A high-granularity digital tracking calorimeter optimized for proton CT. Front. Phys. **8** 568243 (2020). https://www.frontiersin.org/journals/physics/articles/10.3389/fphy.2020.568243/full

[3] A.P. de Haas, et al., The FoCal prototype – an extremely fine-grained electromagnetic calorimeter using CMOS pixel sensors. J. Inst. **13**, P01014 (2018). https://doi.org/10.1088/1748-0221/13/01/P01014

[4] ALICE collaboration, The ALPIDE pixel sensor chip for the upgrade of the ALICE Inner Tracking System. Nucl. Instrum. Meth. A **845** 583 (2017). https://doi.org/10.1016/j.nima.2016.05.016

[5] S. Spannagel, et al., Allpix2: A Modular Simulation Framework for Silicon Detectors. Nucl. Instrum. Meth. A **901** 164 (2018). https://doi.org/10.1016/j.nima.2018.06.020

[6] J. Alme, et al., Performance of the electromagnetic pixel calorimeter prototype EPICAL-2. J. Inst. **18**, P01038 (2023). https://doi.org/10.1088/1748-0221/18/01/P01038.

[7] T. Peitzmann, et al., Results from the EPICAL-2 ultra-high granularity electromagnetic calorimeter prototype. Nucl. Instrum. Meth. A **1045** 167539 (2023). https://doi.org/10.1016/j.nima.2022.167539